Effect of gravity-induced convection on crystal growth process

Toru Maekawa†,Keisuke Ikegami†,Tomoki Tadokoro†,Yoshihiro Sugiki†
Satoshi Matsumoto††

† Toyo University

†† National Space Development Agency of Japan

We investigate the possibility of growing a uniform InAs-GaAs binary compound semiconductor by the Travelling Liquidus Zone (TLZ) method numerically. We focus on buoyancy convection and supercooling induced in the solution in the first half of this report and the crystal growth process under microgravity conditions in the latter half. We find that strong convection and supercooling are induced in the solution under terrestrial gravity conditions, whereas convection is reduced remarkably and an almost diffusion limited crystal growth process is realised by the TLZ method under 1 μg conditions.

1. Introduction

One of the factors which determine the quality of grown crystals may be convective instabilities induced in the melt or solution during the crystal growth process. Growing a multi-component semiconductor crystal which has a uniform composition is especially difficult from both fluid dynamical and thermodynamical points of view [1-6]. Therefore, microgravity experiments of crystal growth have been intensively carried out in recent years utilising microgravity experimental facilities such as drop towers, aircrafts, rockets, space shuttles and satellites, in order to reduce buoyancy convection and grow high-quality crystals [7,8].

Although it is commonly believed that the quality of crystals is directly related to convection induced in the melt or solution, the effect of convection on the crystal growth process is not yet completely understood. It is impossible to grow high-quality compound crystals by experience, unlike single-component crystals. There are two main points which make the growth of multi-component crystals more difficult and complicated compared to the growth of single-component crystals: (1) the shape and movement of the solution–crystal interface are determined by the concentration field in addition to the velocity and temperature fields. The interfacial temperature and concentration of the solute vary along the solution–crystal interface. Note that in the case of single-component crystals, the interfacial temperature is the melting temperature and therefore is constant along the interface. (2) The concentration of the solute at the crystal side of the interface is different from that at the solution side of the interface, which is determined by the liquidus and solidus curves on the phase diagram. Solute is ejected from the crystal into the solution and latent heat is released as phase transition progresses. Since the concentration becomes high near the interface in the solution, supercooling tends to occur, which may cause polycrystallisation.

There is a demand for single high-quality compound crystals to be grown as future materials for fast and efficient electronic or opt-electronic devices [9]. $In_XGa_{1-X}As$ has great potential as a future laser since the wavelength can be altered by changing the composition X. In particular, when $X = 0.3$, a laser of wavelength 1.3 μm, which transmits data through a quartz fibre most efficiently, can be produced [9]. However, it is almost impossible to grow large-scale $In_{0.3}Ga_{0.7}As$ crystals on earth due to strong buoyancy convection and sedimentation. Note that the gap between the solidus and liquidus curves is very wide

This document is provided by JAXA.

at $X = 0.3$ (see figure1), which makes crystal growth extremely difficult.

Generally speaking, when the initial concentration distribution of the solute is uniform throughout the solution, the compositions of the grown crystal are not uniform. If the initial concentration of the solute has a positive gradient in the solution towards the growing crystal, a crystal of uniform compositions may grow [10,11]. We have investigated the crystal growth process by the Bridgman method, imposing the concentration distribution of InAs in the InAs-GaAs solution initially, but found that the concentration field and the crystal interface are seriously deformed by buoyancy convection even under 1 μg conditions [12,13]. Based on the above result, Kinoshita *et al.* [14] proposed a new crystal growth method called the Travelling Liquidus Zone (TLZ) method, which is summarized as follows: (1) InGaAs is grown under 1g conditions. In this case, the concentration distribution of InAs in the grown crystal is not uniform. (2) A part of the terrestrially grown crystal is cut and sandwiched between the seed and feed crystals. The concentration of InAs in the seed crystal is 0.3. (3) The middle part of the crystal is heated to become a solution and crystal is grown by the zone method, instead of the Bridgman method, in microgravity, in which case a linear concentration distribution may be established in the solution and therefore a diffusion limited crystal growth process may be realised. Since crystal grows spontaneously in this case, a crystal of uniform compositions may be produced by setting the heater speed at the spontaneous crystal growth rate.

In this report, we investigate the effect of the level of gravitational acceleration on the crystal growth process, focusing on (1) supercooling induced in the solution by buoyancy convection and (2) the growth rate and interfacial shape of grown crystals. In section 2, we explain the governing equations and calculation method. In section 3, we analyse the relation between buoyancy convection and supercooling induced in the solution. In section 4, we investigate the motion of fine particles in the solution. In section 5, we analyse the crystal growth process by the zone method. In the final section, we summarise the result which we obtained in this study.

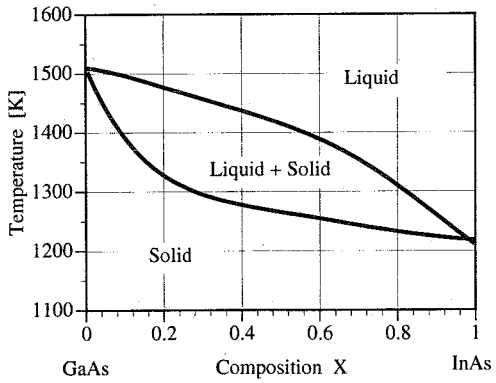

Figure 1 Pseudo-binary phase diagram of $In_XGa_{1-X}As$.

2. Governing equations and calculation method

In this section, we show the governing nondimensional equations in the solution and crystal and explain a method for estimating the movement and shape of the solution–crystal interface. The coordinate x_i, time t, pressure p, velocity v_i and temperature T are nondimensionalised as follows:

$$X_i \equiv \frac{x_i}{L},\quad \tau \equiv \frac{t}{L^2/\nu_L},\quad U_i \equiv \frac{u_i}{\nu_L/L},$$
$$P \equiv \frac{p}{\rho_0 \nu_L^2/L^2},\quad \theta \equiv \frac{T-T_f}{q_0 L/\lambda_L} \text{ or } \equiv \frac{T-T_c}{T_h-T_c}, \tag{1}$$

where L, ν, ρ_0, q_0 and λ are, respectively, the characteristic length, the kinematic viscosity, the density at reference temperature and concentration, the maximum value of heat flux of the heater and the thermal conductivity. Subscript L and f represent liquid and the melting point of InAs. Note that the temperature is nondimensionalised in different ways depending on the situations and that the concentration of InAs is already nondimensionalised (see figure 1).

2.1 Governing equations in solution

The Boussinesq approximations as applied to the density change, the continuity, the momentum and the heat and concentration transport equations are expressed as follows:

Continuity equation:

$$\frac{\partial U_i}{\partial X_i} = 0. \tag{2}$$

Momentum equation:

$$\frac{\partial U_i}{\partial \tau} + U_j \frac{\partial U_i}{\partial X_j} = -\frac{\partial P}{\partial X_i} + \frac{\partial^2 U_i}{\partial X_j \partial X_j} + \frac{Ra^T}{Pr}\theta_L k_i - \frac{Ra^C}{Sc} C_L k_i, \tag{3}$$

This document is provided by JAXA.

where the buoyancy forces based on both the temperature and concentration differences are taken into account and k_i is the unit vector in the gravitational direction. In the case of the InAs–GaAs system, the density increases with a decrease in temperature and with an increase in the concentration of InAs.

Energy equation:

$$\frac{\partial \theta_L}{\partial \tau} + U_j \frac{\partial \theta_L}{\partial X_j} = \frac{1}{Pr} \frac{\partial^2 \theta_L}{\partial X_j \partial X_j}. \tag{4}$$

Transport equation of concentration of InAs:

$$\frac{\partial C_L}{\partial \tau} + U_j \frac{\partial C_L}{\partial X_j} = \frac{1}{Sc} \frac{\partial^2 C_L}{\partial X_j \partial X_j}. \tag{5}$$

Ra^T, Ra^C, Pr and Sc in the above equations are, respectively, the Rayleigh number based on the temperature, the Rayleigh number based on the concentration, the Prandtl number and the Schmidt number:

$$Ra^T \equiv \frac{\beta g q_0 L^4}{\lambda_L \kappa_L \nu_L}, \quad Ra^C \equiv \frac{\gamma g \Delta C L^3}{D_L \nu_L},$$

$$Pr \equiv \frac{\nu_L}{\kappa_L}, \quad Sc \equiv \frac{\nu_L}{D_L}. \tag{6}$$

where β, g, κ_T, γ and D_L are the temperature coefficient of volume expansion, the gravitational acceleration, the thermal diffusivity, the concentration coefficient of volume expansion and the diffusion coefficient.

2.2 Governing equations in crystal

In the crystal, the governing equations are the heat conduction and concentration diffusion equations since convection does not need to be taken into account.

Heat conduction equation:

$$\frac{\partial \theta_S}{\partial \tau} = \frac{K_{SL}}{Pr} \frac{\partial^2 \theta_S}{\partial X_j \partial X_j}. \tag{7}$$

Diffusion equation:

$$\frac{\partial C_S}{\partial \tau} = \frac{D_{SL}}{Sc} \frac{\partial^2 C_S}{\partial X_j \partial X_j}. \tag{8}$$

Here, subscript S represents solid. K_{SL} is the ratio of the thermal diffusivity of the crystal to that of the solution and D_{SL} is the ratio of the diffusion coefficient in the crystal to that in the solution:

$$K_{SL} \equiv \frac{\kappa_S}{\kappa_L}, \quad D_{SL} \equiv \frac{D_S}{D_L}. \tag{9}$$

2.3 Solution–crystal interface

The temperature and concentration at the solution–crystal interface and the position of the interface are determined by the heat and mass balance at the interface and the liquidus and solidus curves on the phase diagram. The phase diagram of the InAs–GaAs binary system is shown in figure 1 [3].

Heat balance equation:

$$\frac{\partial F^*}{\partial \tau} = \frac{Sf}{Pr} \left\{ -\left(\frac{\partial \theta_L}{\partial X_1} - \frac{\partial F^*}{\partial X_2} \frac{\partial \theta_L}{\partial X_2} \right) + G_{SL} \left(\frac{\partial \theta_S}{\partial X_1} - \frac{\partial F^*}{\partial X_2} \frac{\partial \theta_S}{\partial X_2} \right) \right\}. \tag{10}$$

Mass balance equation:

$$(C_L - C_S) \frac{\partial F^*}{\partial \tau} = \frac{1}{Sc} \left\{ -\left(\frac{\partial C_L}{\partial X_1} - \frac{\partial F^*}{\partial X_2} \frac{\partial C_L}{\partial X_2} \right) + D_{SL} \left(\frac{\partial C_S}{\partial X_1} - \frac{\partial F^*}{\partial X_2} \frac{\partial C_S}{\partial X_2} \right) \right\}. \tag{11}$$

Here, F^* is the position of the solution–crystal interafce nondimensionalised by L. G_{SL} is the ratio of the thermal conductivity of the crystal to that of the solution, and Sf is the Stefan number:

$$G_{SL} \equiv \frac{\lambda_S}{\lambda_L}, \quad Sf \equiv \frac{q_0 L}{\rho_0 L_{SL} \kappa_L}. \tag{12}$$

where L_{SL} is the latent heat per unit volume.

There is one important point which we must take into account: the temperature and concentration are not independent at the solution–crystal interface. The relation between the temperature and the concentration is given by the liquidus and solidus curves on the phase diagram. The temperature changes continuously at the interface and therefore the temperatures θ_L and θ_S are the same at the interface, whereas concentration C_L is different from C_S at the interface. Once the interfacial temperature is assigned, C_L and C_S at the interface are determined by the liquidus and solidus curves:

$$C_I = f_L(\theta_I), \quad C_I = f_L(\theta_I). \tag{13}$$

where functions f_L and f_S represent the liquidus and

This document is provided by JAXA.

Table 1 Physical properties, system dimensions and growth conditions

Kinematic viscosity	ν_L	[$m^2 s^{-1}$]	1.5×10^{-7}
Density	ρ_0	[kg m^{-3}]	6.0×10^4
Thermal conductivity of solution	λ_L	[W $m^{-1} K^{-1}$]	3.0
Thermal conductivity of crystal	λ_S	[W $m^{-1} K^{-1}$]	1.2
Temperature coefficient of volume expansion	β	[K^{-1}]	9.34×10^{-5}
Concentration coefficient of volume expansion	γ	[–]	1.85×10^{-1}
Thermal diffusivity of solution	κ_L	[$m^2 s^{-1}$]	1.1×10^{-5}
Thermal diffusivity of crystal	κ_S	[$m^2 s^{-1}$]	3.0×10^{-6}
Diffusion coefficient of In in solution	D_L	[$m^2 s^{-1}$]	2.0×10^{-8}
Diffusion coefficient of In in crystal	D_S	[$m^2 s^{-1}$]	1.0×10^{-11}
Latent heat	L_{SL}	[J kg^{-1}]	5.0×10^5
Depth of solution and crystal	L	[mm]	2, 10, 15, 20
Width of solution and crystal	W	[mm]	120

solidus curves, respectively. Note that $\theta_L = \theta_S$ at the interface as we mentioned. In the present analysis, we approximate the liquidus and solidus curves, f_L and f_S, by the polynomial functions of the fifth order. Since $\partial F^* / \partial \tau$ is common in equations (10) and (11), the right-hand side of equation (10) is equal to the right-hand side of equation (11) divided by $(C_L\text{-}C_S)$. Therefore, the interfacial temperature can be calculated. The interfacial temperature having been determined, the concentrations at the interface are obtained by equation (13).

2.4 Numerical method and procedure

Since the solution–crystal interface moves and the interfacial shape changes during the crystal growth process, we employ the boundary fit method to solve the governing equations efficiently [15]. The transformed equations are solved by the finite difference method. The time and spatial derivatives are approximated by the first-order explicit formula and the second-order central formula, respectively. Now, we can calculate the crystal growth process, that is, the velocity, temperature and concentration fields and the shape and movement of the solution–crystal interface. The nondimensional parameters are estimated based on the physical properties of InAs and GaAs [16,17], which are summarised in table 1.

3. Convection and supercooling in solution

In this section, we focus on buoyancy convection driven in the InAs-GaAs solution, the model of which is shown in figure 2. The left and right walls correspond to the feed and seed crystals. The temperature and concentration at the liquid side of the left wall are fixed at 1392 K and 0.59, while those at the right wall are 1298 K and 0.83, which are determined by the InAs-GaAs phase diagram. Uniform heat flux is given externally from the top and bottom walls. In this case, the governing equations are equations (2)-(5). Note that the second definition is used for the nondimensional temperature (see equation (1)).

Snapshots of streamlines, isotherms, isoconcentration lines and the degree of supercooling, S, are shown in figure 3 for 1 μg conditions and in figure 4 for 1 g conditions, where the height and width of the solution are 20 mm and S is defined as follows:

$$S \equiv \frac{T - T_{Liquidus}}{T_{Liquidus}} \tag{14}$$

Here, T is the local temperature and $T_{Liquidus}$ is the

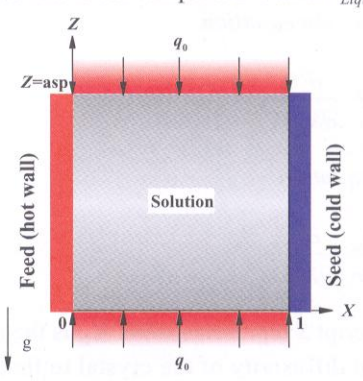

Figure 2 Caluculation model of convection and heat and mass transport in a binary solution

This document is provided by JAXA.

equilibrium temperature corresponding to the liquidus curve (see figure 1). The region where S is negative is supercooled. Weak convection is induced under 1 μg conditions but the temperature field is not seriously disturbed, whereas the concentration field is slightly deformed (figure 3). Although supercooling occurs in the most region of the solution, the degree is not high. On the contrary, strong buoyancy convection is induced under 1 g conditions and, as a result, the temperature and concentration fields are seriously deformed (see figure 4). Strong supercooling is induced near the solution–crystal interface. The time variations of the maximum velicity in the solution is shown in figure 5. In the case of buoyancy convection under 1 μg conditions, the steady-state maximum speed is of the order of 1 μm/s (figure 5 (a)), whereas it is 10 mm/s in the case of 1 g conditions and, furthermore, the speed overshoots in the early stages (figure 5 (b)).

The time variations of the maximum velocity in the solution are shown in figure 6 where the bottom

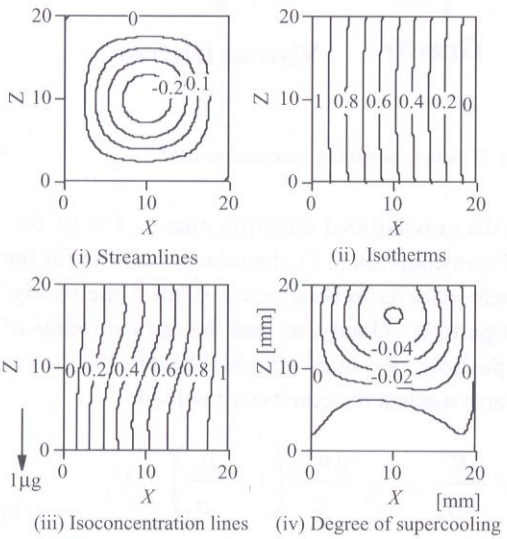

Figure 3 Streamlines, isotherms, isoconcentration lines and degree of supercooling under 1μg conditions. $Ra^T = 0.422$, $Ra^C = 1.18\times10^3$, $Pr = 0.136$, $Sc = 7.5$, $q_0 = 1.0$ kW/m^2, $\tau = 0.2$.

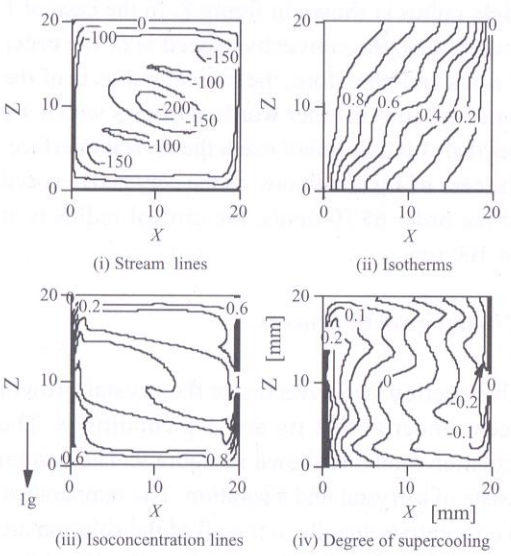

Figure 4 Streamlines, isotherms, isoconcentration lines and degree of supercooling under 1g conditions. $Ra^T = 4.22\times10^5$, $Ra^C = 1.18\times10^9$, $Pr = 0.136$, $Sc = 7.5$, $q_0 = 1.0$ kW/m^2, $\tau = 0.05$.

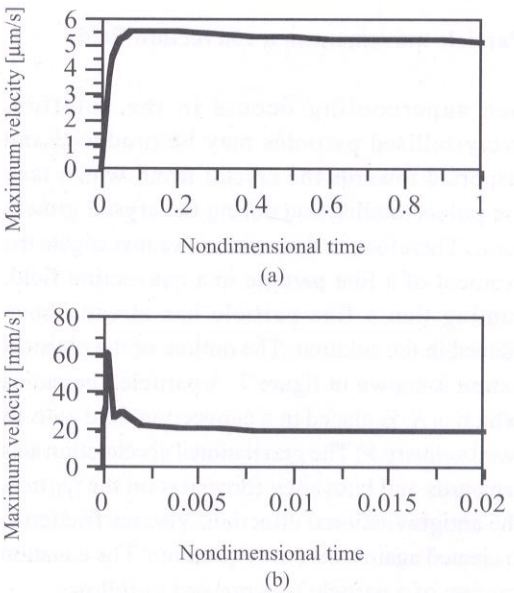

Figure 5 Time variation of maximum velocity. (a) 1g, (b) 1μg.

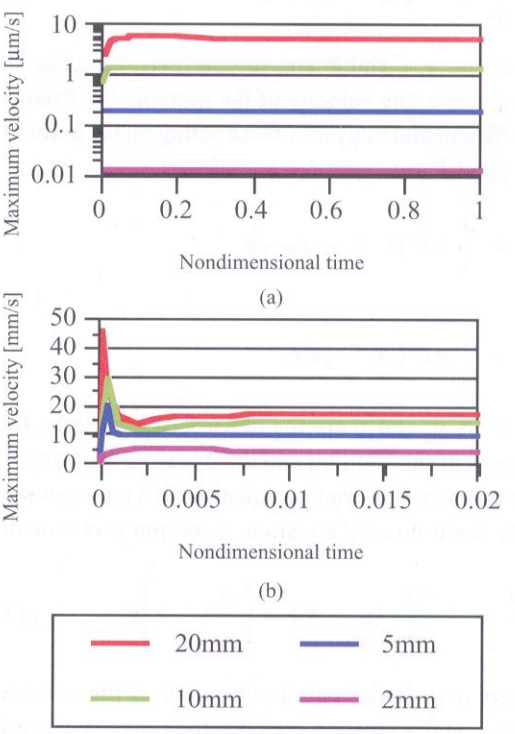

Figure 6 Time variation of maximum velocity. (a) 1g, (b) 1μg.

This document is provided by JAXA.

wall is cooled and heat flux enters from the vertical side walls. In the case of 1 μg conditions, velocity does not overshoot and as the crystal size (the length of cold wall) decreases, the velocity is reduced remarkably (figure 6 (a)). In the case of 1 g conditions, on the other hand, velocity overshoots in the early stages even when the cell is placed vertically, but when the crystal size is shorter than 2 mm, velocity does not overshoot and is reduced greatly (figure 6(b)).

4. Particle movement in a convection field

When supercooling occurs in the solution, polycrystallised particles may be produced and transported towards the crystal front, which may cause polycrystallisation during the crystal growth process. Therefore, in this section, we investigate the movement of a fine particle in a convection field, assuming that a fine particle has already been produced in the solution. The outline of the physical situation is shown in figure 7. A particle, the radius of which is R, is placed in a convection field with an upward velocity V. The gravitational acceleration acts downwards and buoyancy force acts on the particle in the antigravitational direction. Viscous friction is also created against the particle motion. The equation of motion of a particle is expressed as follows:

$$m\frac{d\boldsymbol{u}}{dt} = -\zeta(\boldsymbol{u} - \boldsymbol{V}) + \boldsymbol{F} \tag{15}$$

where m, $\boldsymbol{u}$, ζ and $\boldsymbol{F}$ are, respectively, the mass of the particle, the velocity of the particle, the friction coefficient and buoyancy force acting on the particle. m, ζ and $\boldsymbol{F}$ are expressed as follows:

$$m = \frac{4}{3}\pi R^3\rho,\ \zeta = 6\pi\eta R,$$
$$\boldsymbol{F} = \frac{4}{3}\pi R^3(\rho_s - \rho)\boldsymbol{g}. \tag{16}$$

Here, ρ, ρ_S and η are the density of a particle, the density of the solution and the dynamic viscosity of the solution. Substituting equation (16) into equation (15), the following equation of motion is obtained:

$$\frac{d\boldsymbol{u}}{dt} = -\frac{9\nu}{2R^2}(\boldsymbol{u} - \boldsymbol{V}) + \left(\frac{\rho_s}{\rho} - 1\right)\boldsymbol{g}. \tag{17}$$

where ν is the kinematic viscosity of the solvent. Let us set the situation such that the convective speed

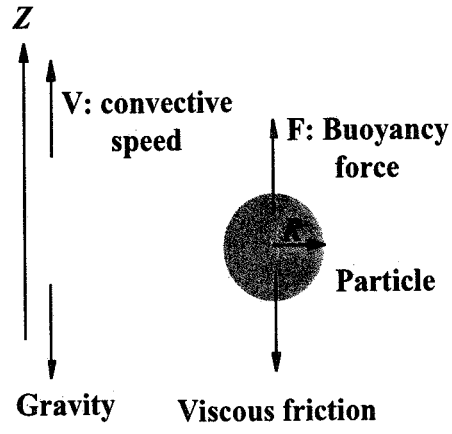

Figure 7 Particle motion in s convective field.

is in the gravitational direction; that is, $\boldsymbol{V} = (0, 0, -V)$. From equation (17), the relaxation time for the particle velocity to become constant, τ, the steady-state particle velocity, u_s, and the critical radius of the particle, R_c, over which the particle moves upwards against the convective velocity:

$$\tau = \frac{2R^2}{9\eta},\ u_s = \frac{2R^2 g}{9}\left(1 - \frac{\rho_s}{\rho}\right) - V, \tag{18}$$
$$R_c = \sqrt{\frac{9\nu V}{2g(1 - \rho/\rho_s)}}$$

The relation between the particle velocity and the particle radius is shown in figure 8. In the case of 1 μg conditions, the convective speed is of the order of 1 μm/s and, therefore, the critical radius is of the order of 1.0 μm. In other words, particles which are larger than 1.0 μm cannot reach the crystal interface. In the case of 1 g conditions, as the convective speed is of the order of 10 mm/s, the critical radius is at most 100 μm.

5. Crystal growth process

In this section, we investigate the crystal growth process under both 1 μg and 1 g conditions. The calculation model is shown in figure 9. The system consists of a crystal and a solution. The temperature and concentration at the left wall of the solution are fixed at 1392 K and 0.59, respectively. Heat flux enters from the top and bottom walls and heat is removed from the right side of the crystal. We

This document is provided by JAXA.

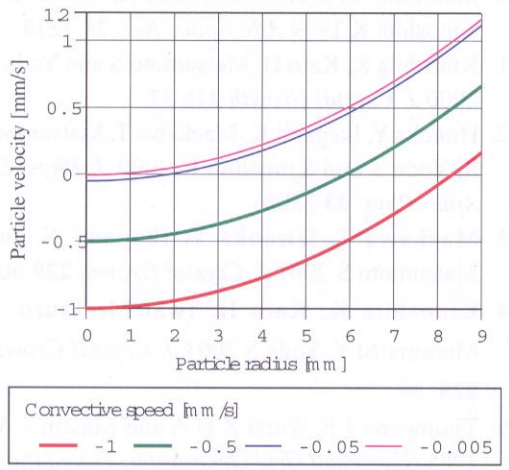

(a)

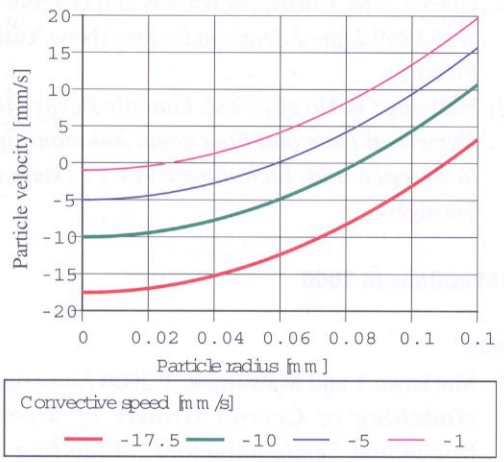

(b)

Figure 8 Dependence of particle velocity on convective speed and particle size (a) 1μg, (b) 1g.

investigate the movement of the solution–crystal interface under both 1 μg and 1 g conditions. Snapshots of streamlines and the shape of the solution–crystal interface are shown in figure 10 and the time variations of the solution–crystal interface are shown in figure 11. Since buoyancy convection is reduced remarkably under 1 μg conditions as shown in section 3, the shape of the solution–crystal interface is convex towards the crystal growth direction, which is favourable for crystal growth, and is almost symmetric. In the case of crystal growth by the zone method under 1 μg conditions, the growth rate is approximately 0.1 mm/s, which is almost the same as that of diffusion growth. In the case of crystal growth under 1 g conditions, on the other hand, strong buoyancy convection is induced and crystal grows very fast. Moreover, the crystal shape becomes asymmetric.

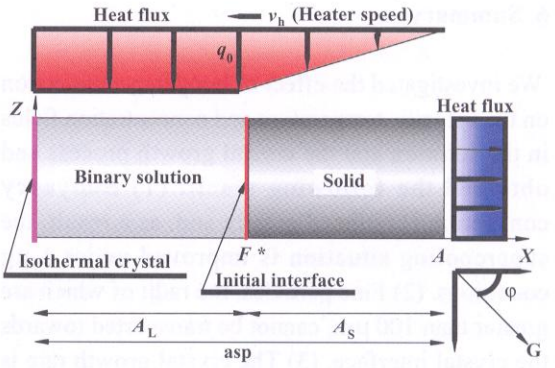

Figure 9 Calculation model of crystal growth of a binary semiconducor.

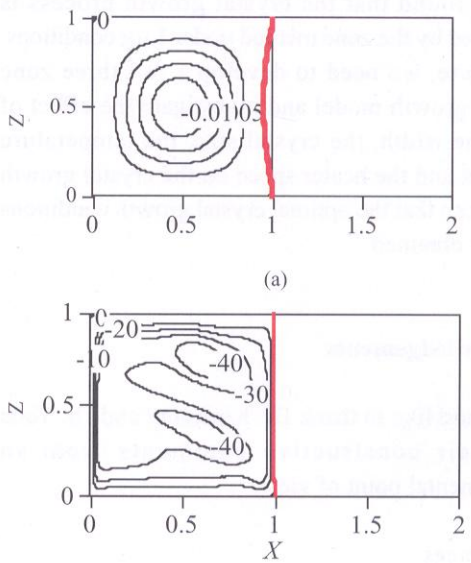

(a)

(b)

Figure 10 Streamlines and interfacial shape. $Pr = 0.136$, $Sc = 7.5$, $Sf = 4.5\times10^{-2}$, ht=0.2mm/h, q_0 =2.0 kW/m^2 (a) 1μg; $Ra^T = 2.96\times10^{-2}$, $Ra^C = 4.94\times10^3$, $\tau = 2.0$. (b) 1g; $Ra^T = 2.96\times10^4$, $Ra^C = 4.94\times10^9$, $\tau = 0.03$.

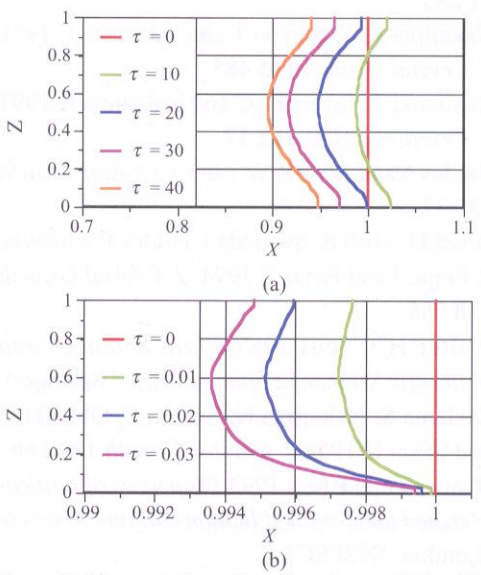

(a)

(b)

Figure 11 Time variation of interface shapes. (a) 1g, (b) 1μg.

This document is provided by JAXA.

6. Summary

We investigated the effect of buoyancy convection on the velocity, temperature and concentration fields in the solution and the crystal growth process and obtained the following result: (1) Buoyancy convection is reduced greatly and, as a result, the supercooling situation is improved under 1 μg conditions. (2) Fine particles, the radii of which are greater than 100 μm, cannot be transported towards the crystal interface. (3) The crystal growth rate is almost the same as that of diffusion growth if we employ the zone method under 1 μg conditions.

We found that the crystal growth process is improved by the zone method under 1 μg conditions. Therefore, we need to develop a full three zone crystal growth model and investigate the effect of the zone width, the crystal size, the temperature gradient and the heater speed on the crystal growth process so that the optimal crystal growth conditions may be obtained.

Acknowledgements

We would like to thank Dr. Kinoshita and Dr. Yoda for their constructive comments from an experimental point of view.

References

1. Kinoshita K and Sugii K 1984 *J. Crystal Growth* **67** 375
2. Kinoshita K and Sugii K 1985 *J. Crystal Growth* **71** 283
3. Nakajima K, Kusunoki T and Takenaka C 1991 *J. Crystal Growth* **113** 485
4. Kusunoki T, Takenaka C and Nakajima K 1991 *J. Crystal Growth* **112** 33
5. Baldus A and Benz K W 1993 *J. Crystal Growth* **130** 37
6. Höschl P, Grill R, Svoboda J, Hlídek P, Moravec P, Franc J and Belas E 1994 *J. Crystal Growth* **138** 956
7. Walter H U (ed) 1987 *Fluid Sciences and Materials Science in Space* (Tokyo: Springer)
8. Kodama S, Nakajima K, Suzuki Y, Ohtsuki O and Sakai H 1988 *J. Crystal Growth* **194** 166
9. Bhattacharya P (ed) 1993 *Properties of Lattice-Matched and Strained Indium Gallium Arsenide* (London: INSPEC)
10. Matumoto S, Maekawa T, Kato K, Yoda S and Kinoshita K 1999 *Adv. Space Res.* **24** 1279
11. Kinoshita K, Kato H, Matsumoto S and Yoda S 2000 *J. Crystal Growth* **216** 37
12. Hiraoka Y, Ikegami K, Maekawa T, Matsumoto S, Yoda S and Kinoshita K 2000 *J. Phys. D: Appl. Phys.* **33** 2508
13. Maekawa T, Hiraoka Y, Ikegami K and Matsumoto S 2001 *J. Crystal Growth* **229** 605
14. Kinoshita K, Kato H, Iwai M, Tsuru T, Muramatsu Y, Yoda S 2001 *J. Crystal Growth* **225** 59
15. Thompson J F, Warsi Z U A and Mastin C W 1985 *Numerical Grid Generation: Foundations and Applications* (New York: Elsevier)
16. Glazov V M, Chizhevskava S N and Glagoleva N N 1969 *Liquid Semiconductors* (New York: Plenum)
17. Hellwege K H (ed) 1982 *Landolt-Börnstein: Numerical Data and Functional Relationships in Science and Technology* vol 17 (Berlin: Springer)

Publications in 2000

Books

1. Maekawa T and Matsumoto T 2000 *Numerical Modelling of Crystal Growth of Binary Compound Semiconductors, Modelling of Transport Phenomena in Crystal Growth* Chapter 4 (J.S. Szmyd (ed)) (Southampton: WIT Press)

Papers

1. Hiraoka Y, Ikegami K, Maekawa T, Matsumoto S, Yoda S and Kinoshita K 2000 *J. Phys. D: Appl. Phys.* **33** 2508
2. Maekawa T, Hiraoka Y, Ikegami K and Matsumoto S 2001 *J. Crystal Growth* **229** 605

International conferences

1. Hiraoka Y, Ikegami K, Maekawa T, Matsumoto S, Yoda S and Kinoshita K 2000 Extended abstract, *The 33rd COSPAR (Committee on Space Research) Scientific Assembly* G0.1-0050, Warsaw, Poland
2. Maekawa T, Hiraoka Y, Ikegami K, Matsumoto S, Yoda S and Kinoshita K 2000 Extended abstract, *The 1st Asian Conference on Crystal Growth and Crystal Technology* T-D-10 380, Sendai, Japan

This document is provided by JAXA.

3. Hiraoka Y, Ikegami K, Maekawa T, Matsumoto S, Yoda S and Kinoshita K 2000 Extended Abstract, *The First International Symposium on Microgravity Research and Applications in Physical Sciences and Biotechnology* 66, Sorrento, Italy

4. Hiraoka Y, Ikegami K, Maekawa T, Matsumoto S, Yoda S and Kinoshita K 2001 *Proc. The First International Symposium on Microgravity Research and Applications in Physical Sciences and Biotechnology* SP-454 vol 1 367-372, ESA

This document is provided by JAXA.